Utah State University
DigitalCommons@USU

Physics Student Research | Physics Student Research

12-13-2010

Uncertainty Associated with Modeling the Global Ionosphere

Janelle V. Jenniges
Utah State University

Ariel O. Acebal
Air Force Institute of Technology

Larry Gardner
Center for Atmospheric and Space Sciences, Utah State University

Robert W. Schunk

Lie Zhu
Utah State University

Follow this and additional works at: https://digitalcommons.usu.edu/phys_stures

 Part of the Oceanography and Atmospheric Sciences and Meteorology Commons, and the Physics Commons

Recommended Citation

Jenniges, J., Acebal, A., Gardner, L., Schunk, R., & Shu, L. (2010, December 13). Uncertainty Associated with Modeling the Global Ionosphere. Poster presented at the American Geophysical Union Fall Meeting, San Francisco, CA.

This Poster is brought to you for free and open access by the Physics Student Research at DigitalCommons@USU. It has been accepted for inclusion in Physics Student Research by an authorized administrator of DigitalCommons@USU. For more information, please contact digitalcommons@usu.edu.

ABS# SA51C-1643
Uncertainty Associated with Modeling the Global Ionosphere

Janelle V. Jenniges
Air Force Institute of Technology
janelle.jenniges@afit.edu

Ariel O. Acebal
Air Force Institute of Technology
ariel.acebal@afit.edu

Larry C. Gardner
Utah State University
Center for Atmospheric and Space Sciences
larry.gardner@usu.edu

Robert W. Schunk
Utah State University
Center for Atmospheric and Space Sciences
robert.schunk@usu.edu

Lie Zhu
Utah State University
Center for Atmospheric and Space Sciences
lie.zhu@usu.edu

ABSTRACT

A study has been conducted of the effect that different physical assumptions have on global models of the electron density distribution. The study was conducted with the Ionosphere Forecast Model (IFM) and the Ionosphere Plasmasphere Model (IPM) developed by Utah State University. Both physics-based, time-dependent, global models use the same empirical models for the neutral atmosphere (MSIS) and neutral wind (Horizontal Wind Model, HWM), but the altitude range, thermal structure, number of ion species, and magnetic field are different. The IFM covers the altitude range from 90-1400 km, calculates the densities for four ions (NO^+, O_2^+, N_2^+, O^+), has a simple prescription for calculating H^+, and is based on a tilted offset dipole magnetic field. The IPM extends from 90-20,000 km, includes six ion species (NO^+, O_2^+, N_2^+, O^+, H^+, He^+), is based on the International Geomagnetic Reference Field (IGRF), and allows for inter-hemisphere flow. Therefore, the comparison of these models will elucidate the quantitative effect of these differences. In addition, simulations were conducted to study the effect of uncertainties in the zonal wind, secondary electron production, O^+/ O collision frequency, tidal structure, and state of plasmasphere refilling. The simulations were conducted for a wide range of solar, seasonal, and geomagnetic activity levels. Quantitative results will be given that establish the importance of the various physical processes.

Baseline Runs

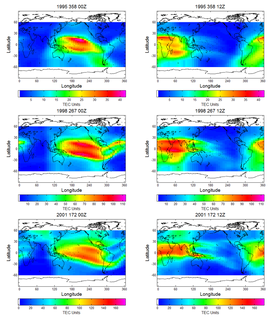

Figure 1. Total electron content for all three cases at 00Z and 12Z

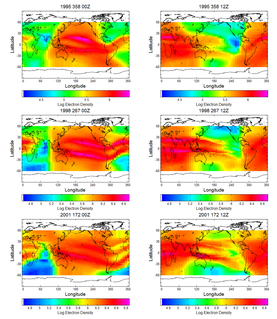

Figure 2. F_2 Peak electron density for all three cases at 00Z and 12Z

Methodology

All three geophysical cases were ran first with the default conditions and then with the adjusted physical parameters. Each parameter was examined independently of the other parameters. The model output from the default run was compared to the adjusted run using an absolute difference, percent change, and a ratio.

Table 1. Geophysical conditions for the three IPM model runs

Case #	Solar Cycle	Season	Year	Day	$F_{10.7}$	K_p	A_p
1	Minimum	December Solstice	1995	358	70	3	15
2	Medium	Fall Equinox	1998	267	140	3	15
3	Maximum	June Solstice	2001	172	220	3	15

Table 2. Adjustments to physical parameters in the IPM

Parameter	Default	Adjustment
O+/O Collision Frequency	Normal	Doubled
Zonal Winds	HWM derived zonal winds	Zonal winds set to zero
Tidal Forcing	No tidal forcing	Tidal forcing included by modulating E x B drift
Secondary Electron Production	Production multiplied by 1.8	Multiplication factor decreased as a linear function of F10.7
Nighttime E x B Drifts	*Scherliess et al* E x B Drifts	Downward E x B drift decreased as a linear function of F10.7

O^+/O Collision Frequency Comparison

Table 3. Percent increase in N_mF_2 due to doubling the O+/O collision frequency

		45N				45S			
		00L	Pre-Sunrise Peak	12L	Daytime Min	00L	Pre-Sunrise Peak	12L	Daytime Min
0E	Case 1	55.76	75.08	8.75	8.59	67.7	75.61	15.76	4.33
	Case 2	40.97	93.26	6.39	6.25	29.4	31.95	12.99	5.86
	Case 3	19.33	53.28	4.86	4.81	20.36	39.4	7.27	-2.04
90E	Case 1	68.94	78.22	13.33	13.03	102.71	142.99	8.97	3.13
	Case 2	33.1	47.98	12.31	9.65	124	178.1	7.89	6.25
	Case 3	23.81	33.73	16.67	14.11	45.52	75.96	12.98	4.03
180E	Case 1	50.66	65.07	9.52	7.44	101.14	140.06	6.87	6.36
	Case 2	24.07	30.64	8.96	6.83	53.21	124.73	3.75	3.61
	Case 3	17.76	33.9	11.98	9.02	46.84	72.65	2.59	-0.99
270E	Case 1	30.86	36.99	10.25	10.22	43.98	76.8	24.76	7.19
	Case 2	75.31	135.16	9.66	9.62	15.11	38.54	9.61	5.79
	Case 3	37.57	89.93	13.81	13.06	48.32	93.26	0.31	-4.16

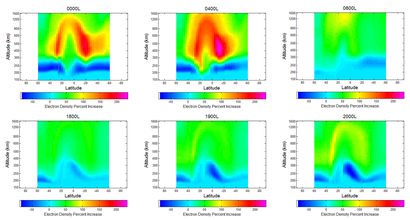

Figure 3. 0°E electron density percent increase for case 1

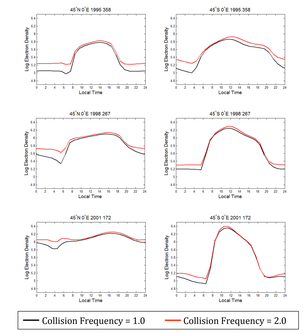

Figure 4. N_mF_2 vs. local time for all three cases

- Doubling the O^+/O collision frequency resulted in increased densities above the F_2 peak and decreased densities below the F_2 peak
- Greatest density increase occurred just before sunrise for all three cases
- Greatest density decrease occurred near local midnight for all three cases
- NmF2 at mid latitude locations was found to increase 30—140% at night

Zonal Wind Comparison

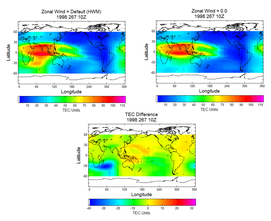

Figure 5. Total electron content for case 2 at 10Z

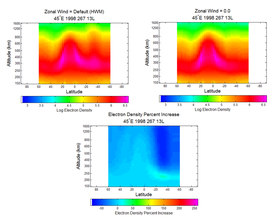

Figure 6. 45°E electron density for case 2 at 13L

- Setting the zonal winds to zero causes the enhancement over Madagascar to decrease for both solar minimum and solar medium from 06Z-14Z
- The maximum decrease in TEC occurs at 10Z for both cases
- Maximum 12 TECU decrease during solar minimum
- Maximum 40 TECU decrease during solar medium

Downward E x B Drift Comparison

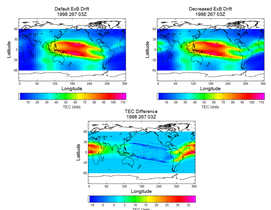

Figure 7. Total electron content for case 2 at 03Z

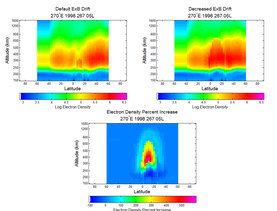

Figure 8. 270°E electron density for case 2 at 05L

- Decreasing the downward E x B drift resulted in increased nighttime low latitude TEC for all three geophysical cases
- The maximum increase in TEC occurs at 05L for all three cases
- Greatest increase of 40 TECU (630%) occurred during solar medium
- 8 TECU increase (480%) during solar minimum
- 30 TECU increase (160%) during solar maximum

Daytime Production Comparison

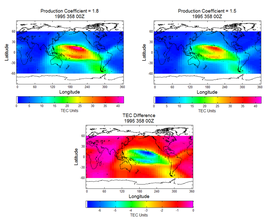

Figure 9. Total electron content for case 1 at 00Z

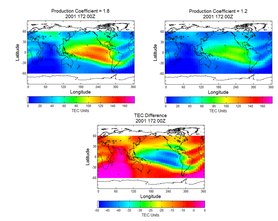

Figure 10. Total electron content for case 3 at 00Z

- Decreasing the daytime production multiplication factor as a linear function of $F_{10.7}$ resulted in decreased TEC values for all three geophysical conditions
- The maximum decrease in TEC occurs at 14L for all three cases
- Greatest decrease of 50 TECYU occurred during solar maximum
- Maximum 7 TECU decrease during solar minimum conditions
- Maximum 30 TECU decrease during solar medium conditions

Tidal Structure Comparison

- Including tidal forcing causes both enhancements and depletions in TEC and 400km N_e as a function of longitude
- The maximum changes in TEC and 400km N_e occur at 13L
- Changes in TEC range from -16% to +23%
- Changes in 400km N_e range from -28% to +44%
- The smallest changes occur during case 3 and the largest changes occur during case 1

Table 4. Maximum percent change in TEC and 400km Ne

	TEC		400km Ne	
	Maximum % Increase	Maximum % Decrease	Maximum % Increase	Maximum % Decrease
Case 1	23	14	44	24
Case 2	21	16	34	28
Case 3	13	11	19	18

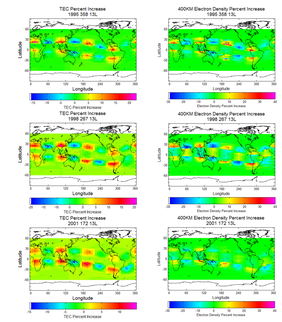

Figure 11. Total electron content and 400km electron density percent increase for all three cases at 13L

Summary and Conclusions

The combination of empirical model output and robust physics in a physics-based model can lead to erroneous and inconsistent features in the model output. These errors are due to the uncertainty in the model parameters and need to be corrected before the model output can be used. This study examined the effects of the uncertainty in five physical parameters in the IPM. These parameters included the O^+/O collision frequency, zonal wind, secondary electron production, nighttime E x B drifts, and tidal structure. The uncertainty for each parameter was evaluated by comparing a default run of the IPM to a run with the parameter adjusted for three different sets of geophysical conditions. The comparisons showed that the effects of these uncertain physical parameters are significant and can be non-linear across both space and time.

It was found that doubling the O^+/O collision frequency increases the peak electron density 30—140% in the equatorial anomalies. The most significant results of setting the zonal winds to zero was a 50% decrease during solar medium equinox near Madagascar. It was found that changes in electron density and TEC are directly proportional to how daytime production is scaled to account for secondary electron production. The result of decreasing the nighttime downward E x B drift was an increase in TEC from 160%—630% at low latitudes depending on season and solar cycle. Finally, tidal forcing was included by modulating the E x B drift and was found to reproduce the four-wave pattern of enhanced TEC at low latitudes. Low latitude TEC increased 15—20% at longitudes centered at 15°E, 110°E, 200°E, and 290°E while decreasing 15—20% at longitudes centered at 60°E, 155°E, 245°E, and 335°E.